Enhanced electromagnetic interference shielding effectiveness of polycarbonate/graphene nanocomposites foamed via 1-step supercritical carbon dioxide process

G. Gedler,[a,b] M. Antunes,[a] J.I. Velasco,[a*] R. Ozisik[b,c*]

[a]Centre Català del Plàstic, Departament de Ciència dels Materials i Enginyeria Metal·lúrgica, Universitat Politècnica de Catalunya · BarcelonaTech (UPC). C/Colom 114, E-08222 Terrassa (Barcelona), Spain.

[b]Department of Materials Science and Engineering and [c]Rensselaer Nanotechnology Center, Rensselaer Polytechnic Institute, Troy, NY 12180, U.S.A.

Abstract: The dielectric and electromagnetic interference (EMI) shielding properties of polycarbonate/graphene nanocomposites foamed using supercritical carbon dioxide were studied as a function of their cellular and composite morphology. Foamed polycarbonate filled with 0.5% (by weight) graphene exhibited enhanced EMI shielding effectiveness, which was found to depend on cellular and composite morphology in a complex manner. Foamed composites presented a maximum specific EMI shielding effectiveness of ~39 dB.cm^3/g, which is approximately 35 times greater than that of unfoamed composite (1.1 dB.cm^3/g). In addition, the relative permittivity was found to increase up to 3.25 times. The results suggest that graphene filled polymer foams can enhance the performance of electronic devices, opening up the possibility of using these materials in electronic applications.

Keywords: Composite foams, graphene, polycarbonate, electromagnetic interference shielding, small angle X-ray scattering, 1-step foaming.

1 Introduction

Materials with electromagnetic interference (EMI) shielding property are needed for protecting electronics particularly those found in strategic systems such as aircraft, nuclear reactors, transformers, control systems, communication systems, among others [1]. The preparation of EMI shielding materials based on polymer composites have been getting increased attention in the academia and industry compared to conventional metal-based materials due to their ease of manufacturing, lightweight and low cost.

Foaming can further lower the weight of polymer-based materials. For example, polycarbonate (PC) is commonly used polymer but its foams have limited industrial use [2] due to the inherent reduction of mechanical properties due to foaming. Two possible routes were proposed to address this problem: controlling the cellular structure, which was shown to play a major role on the final foam properties [3-4] or reinforcing the polymer matrix with fillers, particularly nanofillers [5]. Recent research showed that one can both control the cellular structure and reinforce the polymer matrix by using nanofillers along with supercritical fluid assisted foaming because nanofillers not only act as reinforcing agents but also as nucleation agents during supercritical foaming process [6]. Most importantly, the use of different types of nanofillers can promote control of multiple properties. Nanofillers could also be surface modified with various chemicals or polymer chains to provide additional benefits. For example, recent studies showed that use of conductive polymer coated nanofillers led to substantial enhancement electrical conductivity of polycarbonate [7-8] that could result in enhancement of EMI shielding properties.

Graphene is an extremely attractive material because of the mechanical, thermal and electrical properties that it offers [9-11] Although the incorporation of graphene into polymers is the focal point of many scientific studies, many issues remain to be explored, and only a limited number of studies exist that utilize it in polymer foam based EMI materials. For instance, it has been reported that the foaming process itself can promote ordering of polymer chains [12-13], which could then promote the orientation of nanoparticles. It has been shown that the creation of a cellular structure in composite materials (by means of a foaming process) enhanced electrical conductivity through a tunnelling-like mechanism because of reduced distance between fillers [14]. It has also been stated that the enhancement of electrical conductivity of materials leads to

improved electromagnetic interference shielding [15-18], however, alignment of conductive fillers could have an adverse effect on electromagnetic interference shielding [19]. EMI shielding effectiveness (SE) of 20 dB was reported for epoxy/graphene composites [20] (containing 15% graphene by weight) and 17-21 dB for polyimide/graphene composites [21-22]. The orientation of graphene nanosheets on cell walls due to foaming was suggested as being beneficial for EMI shielding effectiveness [23]. Yang et al. [15] suggested that specific EMI shielding effectiveness would be a more appropriate metric to report when the shielding performance of polymer foams is compared to that of typical metals. For example, Zhang et al. [18] reported specific EMI shielding effectiveness values ranging between 17-25 $dB.cm^3/g$ in the frequency range of 8-12 GHz for poly(methyl methacrylate)/graphene foams containing 1.8% (by volume) graphene.

Absorption was suggested as the primary EMI shielding mechanism in polymer/graphene foams [21] because of large cell-polymer surface area and large specific surface area of well-dispersed graphene sheets. However, materials with good EMI reflection property have been proposed for applications involving radio wave reflection, for example, to be used as lateral guidance for automobiles for enhancing traffic safety particularly at intersections. This method of lateral guidance is much less expensive than the use of magnets embedded along the length of traffic lanes [24]. Recently we prepared PC/graphene composite foams following a 2-step method [25] and later reported the EMI shielding behavior of these materials with low relative densities ranging from 0.14 to 0.28 where the main shielding mechanism exhibited was reflection [26].

In the current study, the electrical conductivity, relative permittivity and electromagnetic interference shielding effectiveness of polycarbonate/graphene composite foams prepared in a single step with relative densities ranging from 0.34 to 0.79 were investigated as a function of polymer nanocomposite morphology and foam cellular structure.

2 Experimental

2.1 Materials

Bisphenol A polycarbonate (Lexan 123R, supplied by SABIC; Sittard, Netherlands) had a density of 1.2 g/cm^3 and a melt flow index of 17.5 dg/min (measured at 300 ºC and with 1.2 kg weight; ISO 1133). Graphene nanoplatelets (GnP, supplied by XG Sciences, Inc.; Michigan, USA) had a bulk density of 2.2 g/cm^3, an average platelet diameter of 15 μm, and platelet

thickness was reported to be 6-8 nm by the manufacturer. In the current study, all polycarbonate/graphene (PC/GnP) composite samples contained 0.5% (by weight) graphene.

2.2 Preparation of composites

Polycarbonate/graphene (PC/GnP) composite samples were prepared by melt compounded using a Brabender Plasti-Corder (Brabender GmbH & Co.) internal mixer. Prior to compounding, PC pellets and GnP nanoplatelets were physically mixed after drying at 110 ºC for 3 hours. The mixture was slowly fed to the internal mixer, which was kept at 180 ºC. The compounding in the internal mixing was done in three stages: at 30 rpm screw speed for two minutes; at 60 rpm for one minute; and finally at 120 rpm for three minutes. The temperature and torque values were monitored during compounding to ensure stability. The PC/GnP melt was removed from the internal mixer and was transferred to a circular cavity mould with a nominal thickness of 3.5 mm and a diameter of 74 mm. The sample was then compression molded in a hot¬plate press (PL 15, IQAP LAP, IQAP Masterbatch Group S.L.; Barcelona, Spain) at 220 ºC with a maximum constant pressure of 4.5 MPa.

2.3 Foaming via 1-step supercritical CO_2 process

Compression moulded polycarbonate/graphene samples were foamed with the use of supercritical carbon dioxide (CO_2) in a 1-step process [27]. Samples were first saturated in supercritical CO_2 up to 120 min at various temperatures (200 213 ºC) and pressures (12.0-16.0 MPa), then they were foamed inside the high-pressure vessel that they were being soaked by releasing pressure at a rate of ~0.3 MPa/s.

2.4 Analysis of cellular morphology

Small and wide angle X-ray scattering (SAXS and WAXS, respectively) experiments were carried out at room temperature using a Nanostar U instrument (Bruker). The X-ray source consisted of a rotating anode with a copper target and 0.1×1.0 mm spot focus filament operated at 50 kV and 24 mA. The detector was placed approximately 105 cm from the sample. WAXS experiments were carried out using a PANalytical diffractometer. CuKα radiation with a wavelength (λ) of 1.54 Å was used at 40 kV and 40 mA at room temperature. Data was collected from 2 to 60º at 0.02º increments. Samples for SAXS and WAXS experiments were prepared by cutting 20×20 mm squares from PC/GnP discs. The square area was selected close to the disc centre but did not include the disc centre. In the case of foamed samples, the thickness of the

sample was reduced to ~5 mm to remove the solid outer skins. In the case of unfoamed samples, the thickness of the samples was ~3.2 mm.

Cellular morphologies were analysed using a JEOL JSM 5610 scanning electron microscope (SEM) operating at 15 kV with a 30 mm working distance. Samples were fractured at cryogenic temperatures and were coated with a thin layer of gold using a BAL TEC SCD005 sputter coater in argon atmosphere. The average cell sizes (ϕ) along the disc thickness (vertical direction, ϕ_{VD}) and radial direction (disc width, ϕ_{WD}) were measured using the intercept counting method [28]. Transmission electron microscopy (TEM) experiments were performed using a JEOL JEM 2011 LaB6 operating at 200 kV and using an AMT XR280 side mount camera with samples having 60-80 nm thickness.

2.5 Electrical conductivity measurements

The electrical conductivity of the solid and foamed PC/GnP composites was measured between 10^{-3} and 10^{6} Hz using a Novocontrol high resolution dielectric, conductivity and impedance modular measurement system. A typical sample had a thickness of 1 mm, which was achieved by carefully sanding each sample. The surfaces of the samples were coated with silver paint in order to reduce the interfacial electrical resistance at contacts. Samples were placed in the Novocontrol dielectric spectrometer between electrodes having a 20 mm diameter.

2.6 Electromagnetic interference shielding effectiveness measurements

The electromagnetic interference shielding effectiveness (EMI-SE) measurements were carried out in the X band frequency range (8.0 12.4 GHz) using an Anritsu 37397C vector network analyzer (VNA), which consisted of two test fixture ports connected to two WR-90 coaxial waveguides and a sample holder that was placed between the two waveguides. Samples having a thickness of 2 mm were cut to fit into the waveguide sample holder (22.9×10.2 mm). A two port VNA calibration was performed before data collection. Scattering parameters S_{11} (forward reflection coefficient) and S_{21} (forward transmission coefficient) were collected to calculate the electromagnetic interference shielding effectiveness.

3 Results and Discussion

3.1 Cellular and composite morphology

The effect of foaming processes on exfoliation, dispersion and distribution of graphene particles was investigated via transmission electron microscopy (TEM). It was found that the 1-step

foaming method led to improved dispersion and distribution of graphene platelets. For example, foamed composite sample PC 05GnP6 (Figure 1a) presented thinner graphene platelets compared to unfoamed composite PC 05GnP (Figure 1b). The influence of various process parameters such as saturation temperature, pressure, and duration on the cellular morphology of foamed samples is displayed in Table 1. The dispersion/exfoliation is believed to be the result of strong attractive interaction of CO_2 molecules and the graphitic structure [29-30]. Specifically, it is suggested that during the dissolution stage, CO_2 molecules interact with the graphitic structure and diffuse in between graphene sheets. Subsequently, during the depressurization stage, CO_2 molecules push graphene layers apart from each other, thereby, promoting dispersion. In addition, extensional flow on the surface of growing bubbles could also promote dispersion by enabling the slipping of graphene layers with respect to each other.

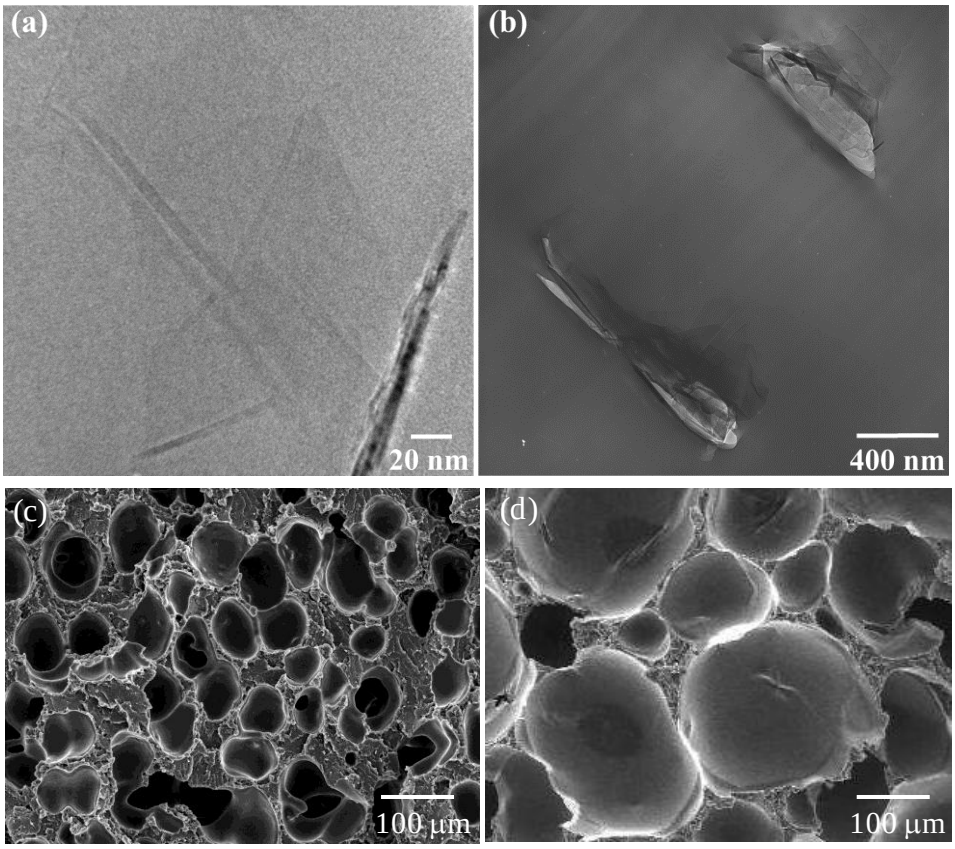

Figure 1. TEM micrographs of (a) foamed (PC 05GnP6) and (b) unfoamed (PC 05GnP) composites. Typical SEM images of cellular structures: (c) PC-05GnP1 and (d) PC-05GnP6.

Cellular morphology of foamed polycarbonate/graphene composites was analyzed via scanning electron microscopy experiments and results were previously reported elsewhere [27, 31],

important parameters are reproduced in Table 1. As expected, cellular morphology strongly depended on graphene concentration, which was kept constant in the current study, and supercritical CO_2 foaming process parameters. Increasing temperature and pressure of CO_2 dissolution/foaming (200 ºC and 13.5 MPa to 213 ºC and 16 MPa) promoted cell growth as can be observed in Figure 1c and 1d. Analysis of the cellular morphology showed that foamed samples had average cell sizes between 60 and 146 μm; cells were distorted such that the average cell aspect ratio (AR) for PC 05GnP1 was greater than one, for PC 05GnP6 it was approximately one, and for the remaining samples they were less than one [27]. In addition, PC/GnP composites soaked in $scCO_2$ without subsequent foaming showed a crystallinity (X) of 22%, however, foaming led to lowered crystallinity (2.4 - 7.3%, Table 1). PC or PC/GnP composites that were not soaked with $scCO_2$ did not show any appreciable crystallinity. It is well know the plasticizing effect of CO_2 in polymers, increasing chain mobility which has been observed to decrease the glass transition temperature [32-35] and increase ordered structures in polymers [31].

Table 1. Foaming process parameters and structural features of polycarbonate, polycarbonate/graphene composites and their foams [31].

Label	T_{sat} (ºC)	P_{sat} (MPa)	t_{sat} (min)	ρ (g/cm^3)	ρ_{rel}	ϕ_{VD} (μm)	ϕ_{WD} (μm)	AR	N_f (cell/cm^3)	X (%)
PC	-	-	-	1.17	-	-	-	-	-	0.0
PC-05GnP	-	-	-	1.14	-	-	-	-	-	0.9
PC-05GnP-CO_2	210	16.0	40	1.19	-	-	-	-	-	22.0
PC-05GnP1	200	13.5	60	0.90	0.79	73.0	58.3	1.25	2.70×10^6	7.3
PC-05GnP2	210	12.0	60	0.67	0.59	86.2	97.3	0.886	1.75×10^6	3.8
PC-05GnP3	205	14.0	160	0.56	0.49	92.9	106.2	0.875	1.10×10^6	6.2
PC-05GnP4	205	15.0	80	0.53	0.46	94.1	111.3	0.845	1.76×10^6	3.7
PC-05GnP5	205	16.0	60	0.43	0.38	97.3	103.9	0.936	1.71×10^6	6.1
PC-05GnP6	213	16.0	40	0.39	0.34	146.6	143.8	1.019	1.04×10^6	2.4

T_{sat}: Saturation (soaking) temperature; P_{sat}: Saturation (soaking) Pressure; t_{sat}: Saturation (soaking) duration; ρ: density; ρ_{rel}: relative density; ϕ_{VD}: Average cell size along the vertical

direction (sample thickness); ϕ_{WD}: Average cell size along the sample width (radial direction); AR: Average cell size aspect ratio (=ϕ_{VD}/ϕ_{WD}); N_f: Cell density; X: Crystallinity as measured via WAXS.

It is believed that (asymmetric) cellular foam morphology, and the presence of crystalline domains and graphene nanoplatelets would all influence the final composite properties. In order to characterize graphene nanoplatelets and crystal distribution, 2 dimensional (2D) SAXS experiments were performed. Results are presented in Figure 2. The solid composite (PC 05GnP) presented a slight anisotropy (see Figure 3a for azimuthal profiles), which could only be due to compression molding because this was the only processing operation performed on this sample after melt mixing. In addition, previous findings showed that this sample did not have any appreciable crystallinity (=0.9% as measured by WAXS) [31]; therefore, the observed anisotropy in the solid sample can only be attributed to orientation of graphene particles as a result of compression molding process. On the other hand, soaked but unfoamed solid sample (PC 05GnP CO_2) showed no anisotropy in SAXS experiments, which suggests that soaking with CO_2 relaxed any existing structural features that was present in this sample following compression molding. It is well known that addition of small molecules (in this case, CO_2) to polymers decreases their glass transition temperature (Tg) and enables relaxation, and this effect was found to be quite prominent during supercritical CO_2 foaming [36]. It is believed that this effect combined with the high soaking pressure and temperature used, and the presence of graphene nanoplatelets led to crystallization of sample PC 05GnP CO_2 [31].

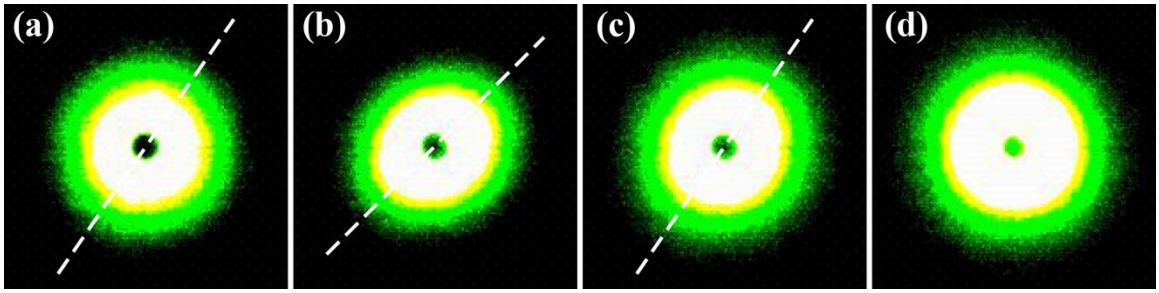

Figure 2. 2D SAXS patterns of (a) unfoamed composite (PC-05GnP), and foamed composites (b) PC-05GnP1, (c) PC-05GnP3, and (d) PC-05GnP6. White dashed lines indicate strongest anisotropy directions.

For the composite foams, the anisotropy was observed to depend on process conditions, and therefore, on foam morphological features such as relative density, average cell size (ϕ_{VD} and ϕ_{WD}), cell density and to any pre-existing structural features. Sample PC-05GnP1, which has the greatest relative density (0.79) and cell aspect ratio (1.25) but the smallest average cell size (66 μm, averaged over ϕ_{VD} and ϕ_{WD}), showed the strongest anisotropy - even stronger than that for PC-05GnP, whereas PC-05GnP6, which has the lowest relative density (0.34) and greatest average cell size (145 μm, averaged over ϕ_{VD} and ϕ_{WD}), showed almost no anisotropy. Experimental results suggest a complex dependence of anisotropy observed in SAXS experiments, even stronger than that of the unfoamed, solid sample (PC 05GnP). Sample PC 05GnP6, which has the lowest relative density (0.34) and an aspect ratio of approximately one but the greatest average cell size (145 μm, averaged over ϕ_{VD} and ϕ_{WD}), showed no anisotropy. Finally, sample PC 05GnP3, which has an intermediate relative density (0.49) and average cell size (100 μm, averaged over ϕ_{VD} and ϕ_{WD}) but an aspect ratio less than one, showed an anisotropy that was greater than that of the unfoamed, solid sample but less than that of PC 05GnP1. Clearly, one parameter that seems to correlate to the observed SAXS anisotropy is the average cell aspect ratio (AR). Anytime, AR deviates from unity, and thereby, cells assume extended shapes, an anisotropy is detected in SAXS experiments. Obviously, if cell growth is isotropic then chain stretching and orientation taking place at growing cell walls (due to elongational flow) will also be isotropic. However, if the cells growth is not isotropic, then chain stretching and orientation at the growing cell walls will not be isotropic. Therefore, it is believed that one structural feature that contributes to the observed anisotropy in 2D SAXS patterns of foamed samples might be due to chain stretching and orientation taking place when cell aspect ratio deviates from one.

However, it is not possible to disregard potential contributions from graphene nanoplatelets or crystals. Even though the solid composite sample soaked in CO_2 without subsequent foaming showed a very high amount of crystallinity (22% measured by WAXS) [31], its 2D SAXS pattern was similar to that of PC-GnP with small anisotropy, and the remnants of this crystallinity were still present in the foamed composites (see Table 1). Therefore, the anisotropy observed in the foamed composite samples could be due to graphene nanoplatelets and/or polymer crystal orientation during foaming but only if cell growth (or sample expansion) is not isotropic. Just recently similar anisotropy has been discussed in composite foams prepared

in 2 steps in which the foams did not present crystallinity [26]. It is possible to detect the distribution of structural heterogeneities in samples from 2D SAXS patterns by integrating the scattering intensity [37]. Figure 3 illustrates the azimuthal profiles of 2D SAXS patterns of the unfoamed PC, the solid composite (PC 05GnP), and the composite foams. Interestingly, it can be seen that graphene nanoplatelet orientation correlates with the average cell aspect ratio: PC 05GnP6 (AR≈1) shows almost no graphene orientation (Figure 3b) and no structural anisotropy (Figure 3a), whereas PC 05GnP1 (AR>1) shows graphene orientation (Figure 3c) and structural anisotropy (Figure 3a).

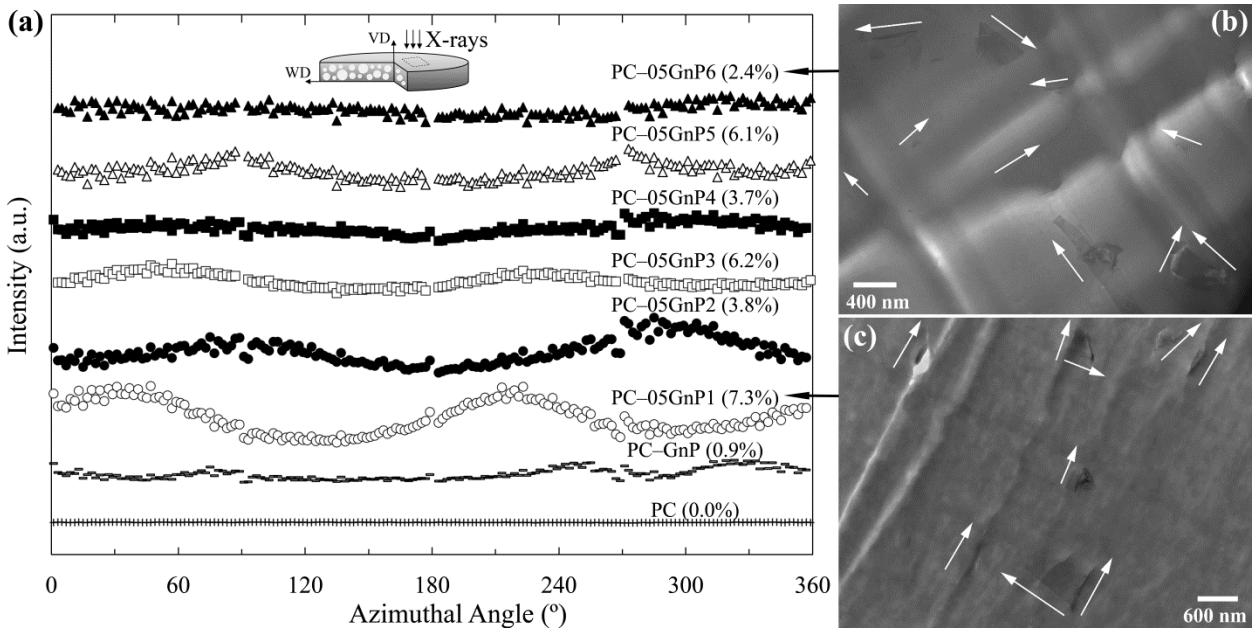

Figure 3. (a) Azimuthal distribution of SAXS intensities for polycarbonate (PC); unfoamed-solid composite (PC-05GnP) and foamed composites (PC 05GnPi, where i=1-6). Numbers in parentheses are crystallinity (*X*) values calculated from WAXD experiments. Example TEM images are provided for (b) PC 05GnP6 (AR=1.019) and (c) PC 05GnP1 (AR=1.25). Arrows in TEM images are added next to graphene nanoplatelets to indicate their orientation with respect to each other.

3.2 Electrical conductivity

The foaming process was found to influence the orientation of graphene particles as discussed previously. This anisotropy in combination with the effect of growing cells on graphene particle distribution (as cells grow they push graphene particles closer to each other within the cell walls, which are also getting thinner with growing cell) might promote the formation of percolation of

graphene particles, and thereby, influence electrical conductivity. Therefore, electrical conductivity measurements were carried out in order to elucidate the possible effects of graphene and foaming process conditions. Although, in general, random orientation of asymmetric particles provides the best chance of forming a percolated network, it is nevertheless important to investigate the effect of graphene orientation and foaming process conditions on electrical conductivity behavior.

The results of the electrical conductivity experiments are presented in Figure 4. Neat polycarbonate (PC) and solid PC/GnP composite showed almost a linear dependence on alternating current (AC) frequency within the range studied. On the other hand, the foamed composites showed frequency independent conductivity (σ_o) at low frequencies and frequency dependant conductivity ($\sigma(\omega)$) at high frequencies. A critical frequency (ω_c) [38] is generally defined to separate the two regions. Strong dispersion of conductivity at low frequencies is one of the characteristic properties of electrical conduction in disordered solids [39]. It has been shown that this dependency is characteristic of hopping in a disordered material where hopping charge carriers are subject to spatially randomly varying energy barriers [40]. This is similar to the fluctuation induced tunnelling model, which was shown to take place in carbon nanotube filled polymers as a result of variations in nanotube-nanotube energy barriers due to local temperature fluctuations [38].

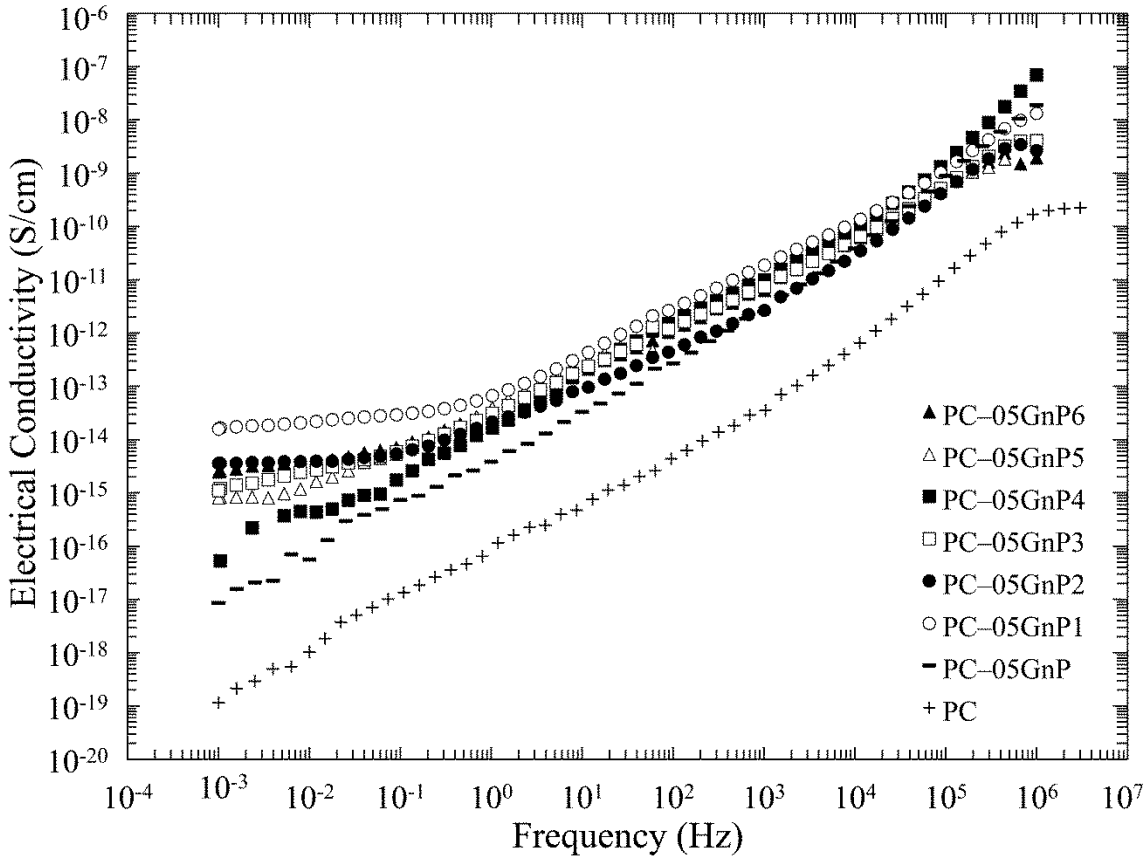

Figure 4. Frequency dependency of AC electrical conductivity for polycarbonate (PC), unfoamed composite (PC-05GnP) and foamed composites.

Although dispersion of graphene particles was shown to improve during cell growth, graphene particles trapped within the cell walls should also be pushed closer to each other as the cell walls get smaller during cell growth [14, 41], the composite foam conductivities did not improve drastically compared to neat PC and solid composite PC 05GnP. At low frequencies, sample PC 05GnP1 showed the greatest electrical conductivity (σ_o = 9 x10 $^{-13}$ S/cm) and critical frequency ($\omega_c \approx 1$ Hz). Interestingly, PC 05GnP1 also showed the strongest anisotropy but more importantly, this sample also contained elongated graphene nanoplatelet structures (Figure 5a) in a manner that creates a path within the composite. It is possible that these structures formed due to shearing of graphene platelets along the vertical direction within the cell walls due to anisotropic cell growth during foaming (AR=1.25 for PC 05GnP1). It should be noted that the vertical direction is also the direction of electrical conductivity measurement. As cell walls get stretched preferentially along the vertical direction, the graphene nanoplatelets experience shear

along the vertical direction. Almost all other foamed composite samples with AR<1 showed lower conductivities and critical frequencies.

Crystallinity did not seem to have any effect on the electrical conductivity. For example, PC 05GnP3 and PC 05GnP4 have similar average cell sizes and cell aspect ratios but have different crystallinity values (6.2% and 3.7%, respectively), however, they showed similar conductivity behavior.

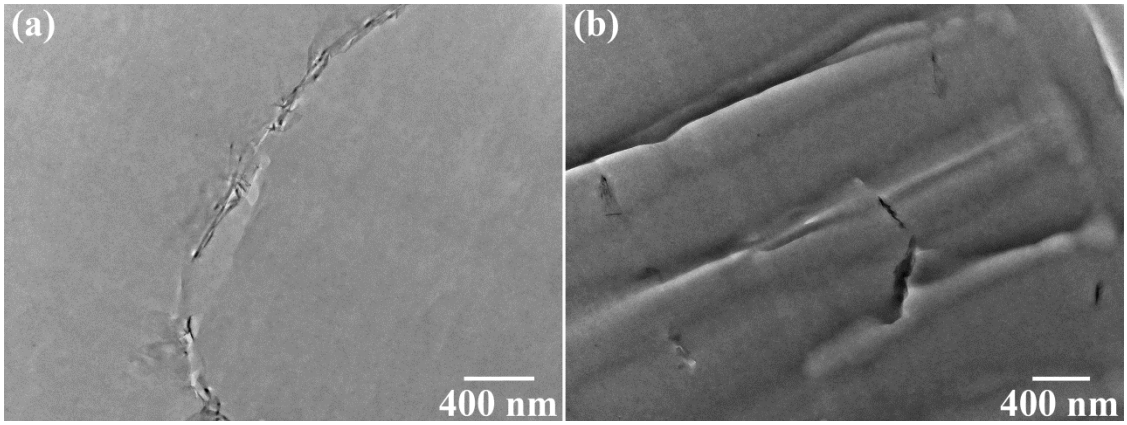

Figure 5. TEM micrographs of foamed composites (a) PC 05GnP1 and (b) PC 05GnP6.

3.3 Relative permittivity

The relative permittivity (ε') was measured in the broadband frequency range of 10^{-3} to 10^{6} Hz at room temperature, and results are presented in Figure 6. Because graphene nanoplatelets did not form a percolated network, a drastic increase in dielectric permittivity was not observed with decreasing frequency [42]. However, foamed composites showed a slightly increasing relative permittivity with decreasing frequency. This is probably related to the fact that polar groups have more time to follow the applied electric field at low frequencies but it might also be related to the presence of graphene nanoplatelets [43-44]. Polymeric systems are essentially insulating materials, and thus, they can be polarized as a response to an applied electrical field. The dielectric relaxations are then a consequence of the various polar groups attempting to follow the applied alternating field [45-46]. However, the presence of conductive particles influences polarization of composite materials by promoting interfacial polarization (Maxwell Wagner Sillar effect) [47-49]. This phenomenon appears in heterogeneous media due to the accumulation of charges at the interfaces and the formation of large dipoles on particles, where the permittivity components are frequency dependent [50]. Interfacial relaxation depends on the conductivity and

permittivity of the constituents of the composite material, and in polymer composites, it occurs in the low frequency region due to the inertia of the formed dipoles. Interfacial polarization results in high values of permittivity (both ε' and ε") that decrease rapidly with frequency [51-52].

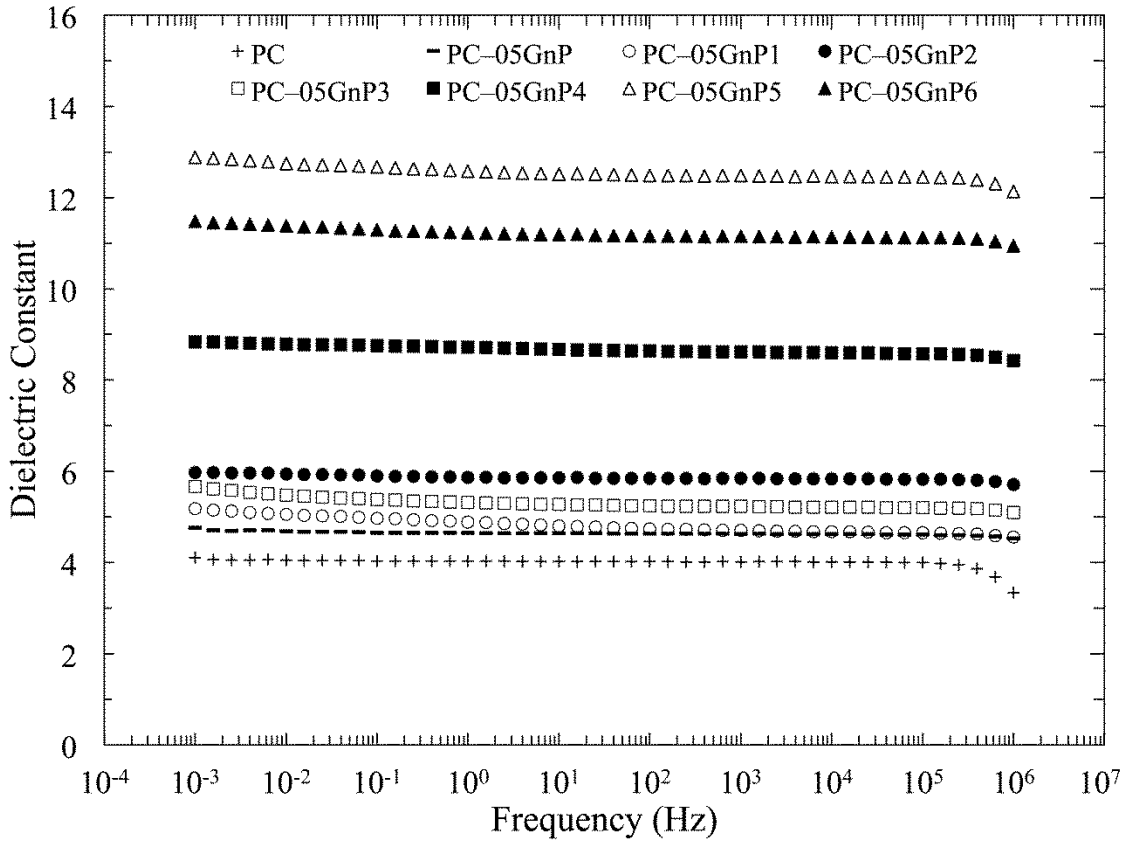

Figure 6. Frequency dependency of absolute relative permittivity for polycarbonate (PC), unfoamed composite (PC 05GnP), and foamed PC/GnP composites.

The dielectric permittivity curves shifted to greater values with the addition of graphene nanoplatelets (compare PC vs. PC 05GnP). Foaming led to further shifting of the permittivity curves to greater values and the greatest permittivity was approximately three times that of neat polycarbonate. The permittivity values increased with decreasing relative density and average cell size, it has been reported that the generation of a cellular structure inside the nanocomposites enhances the dielectric permittivity of polymer composite foams [53]. This observation might be explained by increased conductivity and/or by graphene nanoplatelet dispersion. Although changes in dielectric constant has been attributed to increased electrical conductivity, a direct correlation was not completely observed in the current study; therefore, the permittivity changes

observed in the current study must depend on graphene dispersion. It is known that interfacial polarization density at the polymer filler interface increases with increasing specific surface area of conductive fillers [54], and interfacial polarization can influence the relaxation of polymeric chains and chain segments around the fillers; therefore, samples with better graphene dispersion would have greater dielectric constant. However, opposite behavior was also reported. For example, in clay/polymer nanocomposites, clay layers were shown to restrict the relaxation of polymer chains, and as a result, polymer chains were unable to experience polarization [55]. Therefore, it is obvious that in the current study, the effect of graphene nanoplatelets on chain mobility is not detrimental given the small amount of graphene used.

3.4 Electromagnetic interference shielding effectiveness

The electromagnetic interference (EMI) shielding effectiveness measures a material's ability to attenuate electromagnetic waves. It was converted to dB units by multiplying the logarithm of the forward transmission coefficient (S_{21}) obtained from the vector network analyzer by 20. Figure 7 presents the EMI shielding effectiveness of solid and foamed PC/GnP composites. In general, foamed samples showed enhanced EMI shielding effectiveness compared to solid composite (PC 05GnP) (up to 14 times at ω=8.5 GHz). EMI shielding effectiveness showed a general dependency on foam relative density: EMI SE was found to improve with decreasing foam density. Also, it can be observed that EMI SE decreases with increasing frequency. Even though composites and their foams usually exhibit a fairly frequency-independent EMI SE behavior in the X-band range, there are some reports of frequency-dependent EMI SE behavior, which has been attributed to an inhomogeneous distribution of conductive fillers within the polymer matrix [56-58]. In the current study, similar inhomogeneities could have been caused during formation and growth of the cellular structure, as graphene nanoparticles were being sheared and dispersed within the polycarbonate matrix.

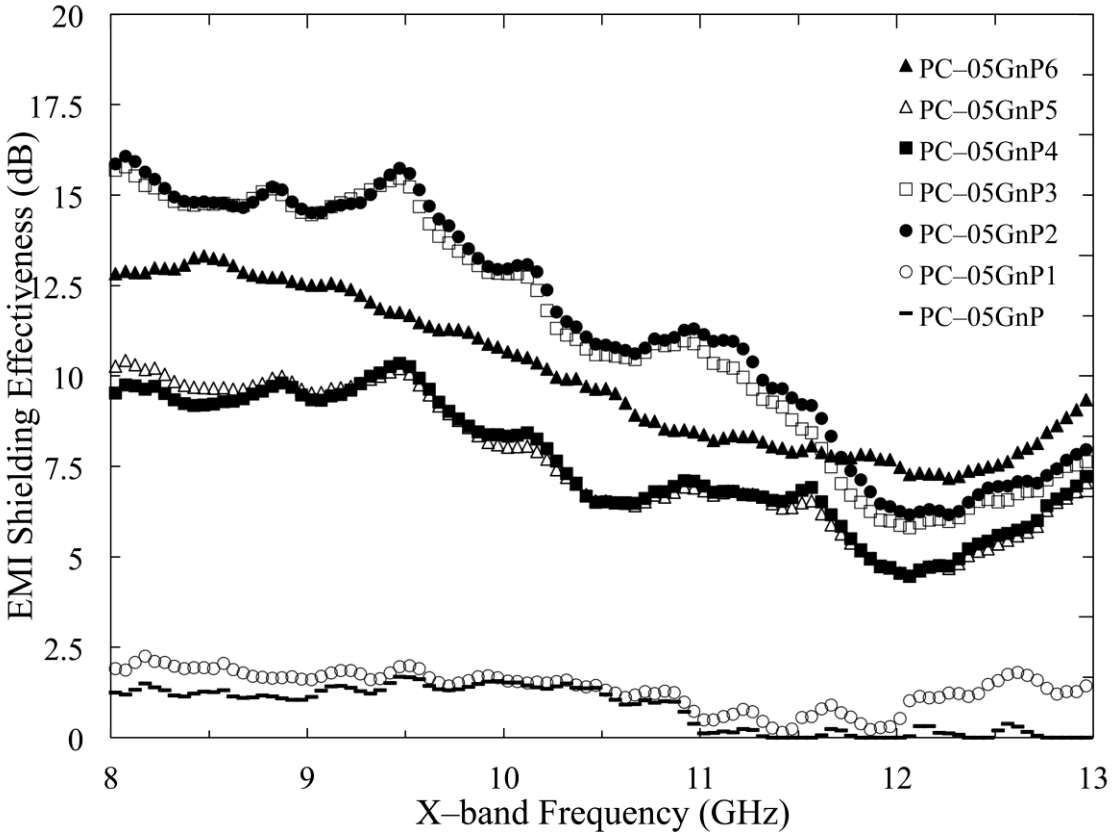

Figure 7. EMI shielding effectiveness of PC/GnP composites and their foams.

It has been suggested that specific EMI shielding effectiveness might be more appropriate when comparing different types of materials such as polymers and polymer foams to metals [15]. The greatest specific EMI shielding effectiveness of foamed samples studied in the current work was found to be ~39 dB·cm^3/g (at 8.5 GHz), which is greater than that of typical metals (i.e., 10 dB·cm^3/g for solid copper [59] commonly used for EMI shielding applications). The maximum EMI shielding effectiveness was found to be ~15 dB (at 8.5 GHz) and it is equivalent to a power attenuation of the incident EM radiation by a factor of ~30, which corresponds to a transmission of ~3.3% [18]. This EMI SE values are slightly higher than PC/graphene foams with considerably lower relative density prepared by the 2-step method [26], in which larger cell sizes promoted higher EMI SE values. However in the composite foams prepared in 1-step, this behavior was not observed. It is well known that the addition of fillers will increase the dielectric permittivity [60-61]. It is possible to state that the enhanced EMI SE is strongly related to the improvement observed in dielectric constant (see Figures 6 and 7). This behavior agrees with previously reported literature findings: EMI shielding (both reflection and absorption

contributions) was found to increase with increasing conductive filler concentration at low concentrations. On the other hand, at high conductive filler concentrations, the absorption contribution was found to increase while the reflection contribution was fund to decrease [60]. In the current study, the observed increase in dielectric constant during foaming could be related to the enhanced dispersion of graphene nanoplatelets taking place during foaming, as previously discussed, rather than to the addition of high amount of filler. Therefore, it can be stated that the synergetic effect of graphene nanoplatelet dispersion during foaming and the formation of the cellular structure moderately improved electrical conductivity but also increased the dielectric constant of the composite foams with low graphene concentration (see Figures 4 and 5), and as a result, leading to enhanced EMI SE.

Three types of mechanisms contribute to the shielding effectiveness of materials: reflection, absorption, and multiple reflection [62]. In foams, reflection is related to impedance mismatch between air (in the cells) and absorber (matrix material) [15, 60, 62], absorption is related to energy dissipation in the absorber, and multiple reflections are considered to be due to scattering effect of inhomogeneities that might exist within the material [18]. To understand which mechanisms are operational in the current work, reflection contribution was calculated for each sample and is presented in Figure 8 as a function of relative density. The sum of absorption and multiple reflection mechanism contributions were calculated by subtracting the reflection from the total shielding effectiveness. The mechanism of shielding for the foamed samples was found to be a combination of reflection and absorption+multiple reflections with absorption+multiple reflection contribution being slightly lower than reflection contribution. Foamed composites display moderate values of electrical conductivity and absorption mechanism is known to be strongly proportional to electrical conductivity [18, 23, 63], therefore, the observed contributions reflect this fact.

It has been stated that foaming facilitates absorption of microwaves because microwaves could be reflected and scattered many times by cell matrix interfaces and nanofillers [64]. With decreasing relative density, reflection and absorption+multiple reflection were found to increase but they all experienced a sudden decrease at the relative density of 0.46 (sample PC-05GnP4) and then continued to increase with decreasing relative density (see Figure 8). The ultimate cause for this behavior should be studied further.

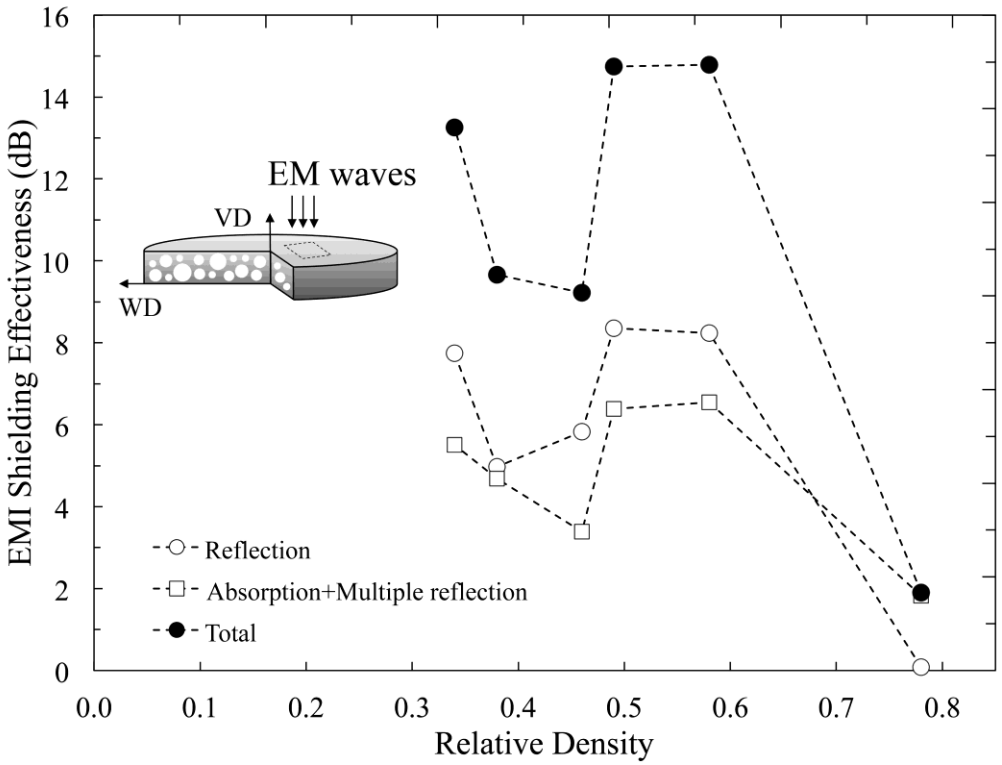

Figure 8. Various shielding contributions to electromagnetic interference (EMI) shielding as a function of relative density for unfoamed and foamed composites at a constant frequency of 8.5 GHz.

4 Conclusions

Electromagnetic interference shielding effectiveness and relative permittivity of polycarbonate (PC) was improved upon addition of graphene nanoplatelets (GnPs). Foaming with supercritical carbon dioxide further enhanced these properties. Electrical conductivity, relative permittivity, and electromagnetic interference shielding were all found to strongly depend on structural and cell morphology, and therefore on foaming process conditions. All three properties showed a complex dependence on structural features and cellular morphology but were mainly affected by the lack of a percolated graphene network even though foaming was found to enhance graphene dispersion in polycarbonate. Electrical conductivity was found to strongly depend on frequency, and electrical conductivity, relative permittivity and electromagnetic shielding effectiveness were greater for foamed composites compared to solid composite and neat polycarbonate. The foam composites displayed specific electromagnetic interference shielding effectiveness up to 39 $dB.cm^3/g$, which is greater than that reported for copper - a material commonly used for

electromagnetic interference shielding applications. This suggests that foamed graphene filled polymer composites with a broad range of densities (higher densities when prepared in 1-step and lower densities when prepared in 2-steps) could be used as electromagnetic shielding materials; however, more studies are needed to control graphene dispersion, distribution, and percolation in these materials.

5 Acknowledgements

The authors would like to acknowledge financial support provided by the Spanish Ministry of Economy and Competitiveness (MAT2014-56213) and the National Science Foundation (CMMI-1200270, DUE-1003574 and DUE-1406405).

6 References

[1] Geetha S, Satheesh Kumar KK, Rao CRK, Vijayan M, Trivedi DC. EMI shielding: Methods and materials—A review. Journal of Applied Polymer Science. 2009;112:2073-86.

[2] Landrock A. Handbook of Plastic Foams. New Jersey: Noyes; 1995.

[3] Yun MS, Lee WI. Analysis of bubble nucleation and growth in the pultrusion process of phenolic foam composites. Composites Science and Technology. 2008;68:202-8.

[4] Guo H, Nadella K, Kumar V. Effect of intrinsic viscosity on solid-state microcellular foaming of polyethylene terephthalate. Journal of Materials Research. 2013;28:2374-9.

[5] Ehrburger-Dolle F, Hindermann-Bischoff M, Livet F, Bley F, Rochas C, Geissler E. Anisotropic Ultra-Small-Angle X-ray Scattering in Carbon Black Filled Polymers. Langmuir. 2000;17:329-34.

[6] Chen L, Rende D, Schadler LS, Ozisik R. Polymer nanocomposite foams. Journal of Materials Chemistry A. 2013;1:3837-50.

[7] Zhou J, Lubineau G. Improving Electrical Conductivity in Polycarbonate Nanocomposites Using Highly Conductive PEDOT/PSS Coated MWCNTs. ACS Applied Materials & Interfaces. 2013;5:6189-200.

[8] Aguilar Ventura I, Zhou J, Lubineau G. Drastic modification of the piezoresistive behavior of polymer nanocomposites by using conductive polymer coatings. Composites Science and Technology. 2015;117:342-50.

[9] Kuilla T, Bhadra S, Yao D, Kim NH, Bose S, Lee JH. Recent advances in graphene based polymer composites. Progress in Polymer Science (Oxford). 2010;35:1350-75.
[10] Katsnelson MI. Graphene: carbon in two dimensions. Materials Today. 2007;10:20-7.
[11] Wang H, Robinson JT, Diankov G, Dai H. Nanocrystal Growth on Graphene with Various Degrees of Oxidation. Journal of the American Chemical Society. 2010;132:3270-1.
[12] Bao J-B, Liu T, Zhao L, Hu G-H, Miao X, Li X. Oriented foaming of polystyrene with supercritical carbon dioxide for toughening. Polymer. 2012;53:5982-93.
[13] Rodríguez-Pérez MA, Campo-Arnáiz RA, Aroca RF, de Saja JA. Characterisation of the matrix polymer morphology of polyolefins foams by Raman spectroscopy. Polymer. 2005;46:12093-102.
[14] Antunes M, Mudarra M, Velasco JI. Broad-band electrical conductivity of carbon nanofibre-reinforced polypropylene foams. Carbon. 2011;49:708-17.
[15] Yang Y, Gupta MC, Dudley KL, Lawrence RW. Novel Carbon Nanotube−Polystyrene Foam Composites for Electromagnetic Interference Shielding. Nano Letters. 2005;5:2131-4.
[16] Yang Y, Gupta MC, Dudley KL, Lawrence RW. A Comparative Study of EMI Shielding Properties of Carbon Nanofiber and Multi-Walled Carbon Nanotube Filled Polymer Composites. Journal of Nanoscience and Nanotechnology. 2005;5:927-31.
[17] Ameli A, Jung PU, Park CB. Electrical properties and electromagnetic interference shielding effectiveness of polypropylene/carbon fiber composite foams. Carbon. 2013;60:379-91.
[18] Zhang H-B, Yan Q, Zheng W-G, He Z, Yu Z-Z. Tough Graphene−Polymer Microcellular Foams for Electromagnetic Interference Shielding. ACS Applied Materials & Interfaces. 2011;3:918-24.
[19] Arjmand M, Apperley T, Okoniewski M, Sundararaj U. Comparative study of electromagnetic interference shielding properties of injection molded versus compression molded multi-walled carbon nanotube/polystyrene composites. Carbon. 2012;50:5126-34.
[20] Liang J, Wang Y, Huang Y, Ma Y, Liu Z, Cai J, et al. Electromagnetic interference shielding of graphene/epoxy composites. Carbon. 2009;47:922-5.
[21] Shen B, Zhai W, Lu D, Zheng W, Yan Q. Fabrication of microcellular polymer/graphene nanocomposite foams. Polymer International. 2012;61:1693-702.

[22] Li Y, Pei X, Shen B, Zhai W, Zhang L, Zheng W. Polyimide/graphene composite foam sheets with ultrahigh thermostability for electromagnetic interference shielding. RSC Advances. 2015;5:24342-51.
[23] Ling J, Zhai W, Feng W, Shen B, Zhang J, Zheng Wg. Facile Preparation of Lightweight Microcellular Polyetherimide/Graphene Composite Foams for Electromagnetic Interference Shielding. ACS Applied Materials & Interfaces. 2013;5:2677-84.
[24] Chung DDL. Carbon materials for structural self-sensing, electromagnetic shielding and thermal interfacing. Carbon. 2012;50:3342-53.
[25] Gedler G, Antunes M, Velasco JI. Effects of graphene nanoplatelets on the morphology of polycarbonate–graphene composite foams prepared by supercritical carbon dioxide two-step foaming. The Journal of Supercritical Fluids. 2015;100:167-74.
[26] Gedler G, Antunes M, Velasco JI, Ozisik R. Electromagnetic shielding effectiveness of polycarbonate/graphene nanocomposite foams processed in 2-steps with supercritical carbon dioxide. Materials Letters. 2015;160:41-4.
[27] Gedler G, Antunes M, Realinho V, Velasco JI. Novel polycarbonate-graphene nanocomposite foams prepared by CO2 dissolution. IOP Conference Series: Materials Science and Engineering. 2012;31:012008.
[28] Sims G, Khunniteekool C. Cell Size Measurement of Polymeric Foams. Cell Polym. 1994;13:137-46.
[29] Montoya A, Mondragón F, Truong TN. CO2 adsorption on carbonaceous surfaces: a combined experimental and theoretical study. Carbon. 2003;41:29-39.
[30] Ghosh A, Subrahmanyam KS, Krishna KS, Datta S, Govindaraj A, Pati SK, et al. Uptake of H2 and CO2 by Graphene. The Journal of Physical Chemistry C. 2008;112:15704-7.
[31] Gedler G, Antunes M, Velasco JI. Graphene-induced crystallinity of bisphenol A polycarbonate in the presence of supercritical carbon dioxide. Polymer. 2013;54:6389-98.
[32] Guo H, Kumar V. Solid-state poly(methyl methacrylate) (PMMA) nanofoams. Part I: Low-temperature CO2 sorption, diffusion, and the depression in PMMA glass transition. Polymer. 2015;57:157-63.
[33] Weller JE, Kumar V. Solid-state microcellular polycarbonate foams. I. The steady-state process space using subcritical carbon dioxide. Polymer Engineering & Science. 2010;50:2160-9.

[34] Guo H, Nicolae A, Kumar V. Solid-state microcellular and nanocellular polysulfone foams. Journal of Polymer Science Part B: Polymer Physics. 2015;53:975-85.
[35] Guo H, Kumar V. Effect of glass transition temperature and saturation temperature on the solid-state microcellular foaming of cyclic olefin copolymer. Journal of Applied Polymer Science. 2015;132:n/a-n/a.
[36] Rende D, Schadler LS, Ozisik R. Controlling Foam Morphology of Poly(methyl methacrylate) via Surface Chemistry and Concentration of Silica Nanoparticles and Supercritical Carbon Dioxide Process Parameters. Journal of Chemistry. 2013;2013:13.
[37] Somani RH, Yang L, Hsiao BS. Precursors of primary nucleation induced by flow in isotactic polypropylene. Physica A: Statistical Mechanics and its Applications. 2002;304:145-57.
[38] Kilbride BE, Coleman JN, Fraysse J, Fournet P, Cadek M, Drury A, et al. Experimental observation of scaling laws for alternating current and direct current conductivity in polymer-carbon nanotube composite thin films. Journal of Applied Physics. 2002;92:4024-30.
[39] Dyre JC, Schrøder TB. Universality of ac conduction in disordered solids. Reviews of Modern Physics. 2000;72:873-92.
[40] Dyre JC. The random free-energy barrier model for ac conduction in disordered solids. Journal of Applied Physics. 1988;64:2456-68.
[41] Antunes M, Velasco JI. Multifunctional polymer foams with carbon nanoparticles. Progress in Polymer Science. 2014;39:486-509.
[42] Pötschke P, Abdel-Goad M, Alig I, Dudkin S, Lellinger D. Rheological and dielectrical characterization of melt mixed polycarbonate-multiwalled carbon nanotube composites. Polymer. 2004;45:8863-70.
[43] Schaefer DW, Justice RS. How Nano Are Nanocomposites? Macromolecules. 2007;40:8501-17.
[44] Barrau S, Demont P, Peigney A, Laurent C, Lacabanne C. DC and AC Conductivity of Carbon Nanotubes−Polyepoxy Composites. Macromolecules. 2003;36:5187-94.
[45] Nogales A, Denchev Z, Ezquerra TA. Influence of the Crystalline Structure in the Segmental Mobility of Semicrystalline Polymers: Poly(ethylene naphthalene-2,6-dicarboxylate). Macromolecules. 2000;33:9367-75.
[46] Okrasa L, Boiteux G, Ulanski J, Seytre G. Molecular relaxation in anisotropic composites based on (hydroxypropyl)cellulose and acrylic polymer. Polymer. 2001;42:3817-25.

[47] Tsangaris GM, Psarras GC. The dielectric response of a polymeric three-component composite. Journal of Materials Science. 1999;34:2151-7.
[48] Pelster R, Marquardt P, Nimtz G, Enders A, Eifert H, Friederich K, et al. Realization of dielectrics with a metal-like dispersion. Physical Review B. 1992;45:8929-33.
[49] Perrier G, Bergeret A. Polystyrene–glass bead composites: Maxwell–Wagner–Sillars relaxations and percolation. Journal of Polymer Science Part B: Polymer Physics. 1997;35:1349-59.
[50] Sillars RW. The properties of a dielectric containing semiconducting particles of various shapes. Institution of Electrical Engineers - Proceedings of the Wireless Section of the Institution1937. p. 139-55.
[51] Tsangaris GM, Psarras GC, Kouloumbi N. Electric modulus and interfacial polarization in composite polymeric systems. Journal of Materials Science. 1998;33:2027-37.
[52] Psarras GC, Manolakaki E, Tsangaris GM. Electrical relaxations in polymeric particulate composites of epoxy resin and metal particles. Composites Part A: Applied Science and Manufacturing. 2002;33:375-84.
[53] Ameli A, Wang S, Kazemi Y, Park CB, Pötschke P. A facile method to increase the charge storage capability of polymer nanocomposites. Nano Energy. 2015;15:54-65.
[54] Kim J-Y, Kim T, Suk JW, Chou H, Jang J-H, Lee JH, et al. Enhanced Dielectric Performance in Polymer Composite Films with Carbon Nanotube-Reduced Graphene Oxide Hybrid Filler. Small. 2014;10:3405-11.
[55] Jose AJ, Alagar M, P. Thomas S. Preparation and Characterization of Organoclay Filled Polysulfone Nanocomposites. Materials and Manufacturing Processes. 2011;27:247-54.
[56] Thomassin J-M, Jérôme C, Pardoen T, Bailly C, Huynen I, Detrembleur C. Polymer/carbon based composites as electromagnetic interference (EMI) shielding materials. Materials Science and Engineering: R: Reports. 2013;74:211-32.
[57] Anupama J, Anil B, Rajvinder S, Alegaonkar PS, Balasubramanian K, Suwarna D. Graphene nanoribbon?PVA composite as EMI shielding material in the X band. Nanotechnology. 2013;24:455705.
[58] Das NC, Chaki TK, Khastgir D, Chakraborty A. Electromagnetic interference shielding effectiveness of conductive carbon black and carbon fiber-filled composites based on rubber and rubber blends. Advances in Polymer Technology. 2001;20:226-36.

[59] Shui X, Chung DDL. Nickel filament polymer-matrix composites with low surface impedance and high electromagnetic interference shielding effectiveness. Journal of Elec Materi. 1997;26:928-34.
[60] Liu Z, Bai G, Huang Y, Ma Y, Du F, Li F, et al. Reflection and absorption contributions to the electromagnetic interference shielding of single-walled carbon nanotube/polyurethane composites. Carbon. 2007;45:821-7.
[61] Ameli A, Nofar M, Park CB, Pötschke P, Rizvi G. Polypropylene/carbon nanotube nano/microcellular structures with high dielectric permittivity, low dielectric loss, and low percolation threshold. Carbon. 2014;71:206-17.
[62] Thomassin J-M, Pagnoulle C, Bednarz L, Huynen I, Jerome R, Detrembleur C. Foams of polycaprolactone/MWNT nanocomposites for efficient EMI reduction. Journal of Materials Chemistry. 2008;18:792-6.
[63] Ameli A, Nofar M, Wang S, Park CB. Lightweight Polypropylene/Stainless-Steel Fiber Composite Foams with Low Percolation for Efficient Electromagnetic Interference Shielding. ACS Applied Materials & Interfaces. 2014;6:11091-100.
[64] Li C, Yang G, Deng H, Wang K, Zhang Q, Chen F, et al. The preparation and properties of polystyrene/functionalized graphene nanocomposite foams using supercritical carbon dioxide. Polymer International. 2013;62:1077-84.

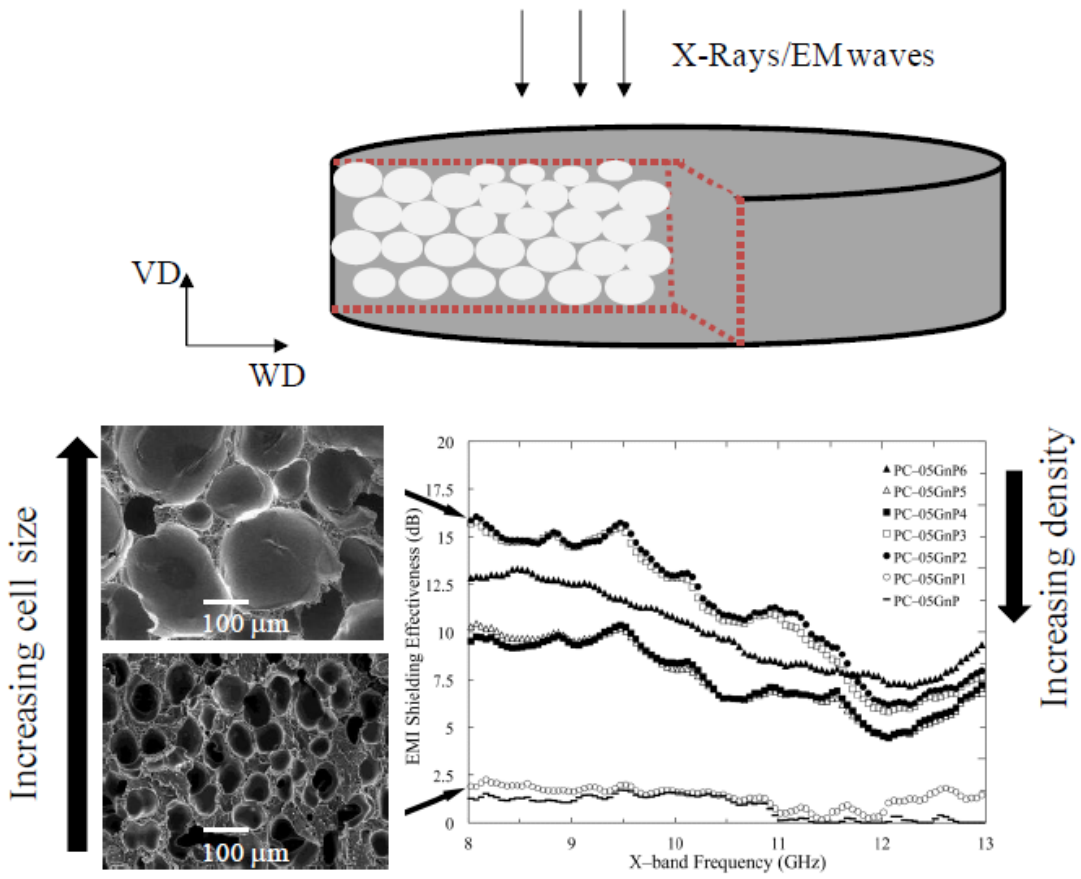

Graphical abstract

Highlights

- Foaming promoted better graphene dispersion/distribution and hence, better EMI shielding.
- Shielding effectiveness increased ~15 times after foaming.
- Maximum specific shielding effectiveness of foamed composites was 39 dB.cm^3/g, 4x that of copper.
- Relative permittivity of PC improved upon foaming and the addition of graphene.
- All EMI shielding mechanism contributed in a similar fashion.